arXiv:1410.5315v1 [physics.acc-ph] 20 Oct 2014

STATUS OF HEAD-ON BEAM–BEAM COMPENSATION IN RHIC *

W. Fischer†, Z. Altinbas, M. Anerella, M. Blaskiewicz, D. Bruno, M. Costanzo, W.C. Dawson, D.M. Gassner, X. Gu, R.C. Gupta, K. Hamdi, J. Hock, L.T. Hoff, R. Hulsart, A.K. Jain, R. Lambiase, Y. Luo, M. Mapes, A. Marone, R. Michnoff, T.A. Miller, M. Minty, C. Montag, J. Muratore, S. Nemesure, D. Phillips, A.I. Pikin, S.R. Plate, P. Rosas, L. Snydstrup, Y. Tan, C. Theisen, P. Thieberger, J. Tuozzolo, P. Wanderer, S.M. White, W. Zhang
BNL, Upton, NY, USA

Abstract

In polarized proton operation, the performance of the Relativistic Heavy Ion Collider (RHIC) is limited by the head-on beam–beam effect. To overcome this limitation, two electron lenses are under commissioning. We give an overview of head-on beam–beam compensation in general and in the specific design for RHIC, which is based on electron lenses. The status of installation and commissioning are presented along with plans for the future.

INTRODUCTION

Head-on beam–beam compensation was first proposed as a four-beam $e^+e^-e^+e^-$ scheme for COPPELIA [1] and implemented for Dispositif de Collisions dans l'Igloo (DCI) [2]. The DCI experience, however, fell short of expectations; luminosities with two, three, or four beams were about the same. The shortfall is generally attributed to coherent beam–beam instabilities [3–5], and head-on beam–beam compensation has not been tested again since.

Nevertheless, various proposals have been made, such as for the SSC [6, 7], Tevatron [8], LHC [6, 7, 9–11], and B-factories [12]. In hadron colliders, the compensation can be achieved by colliding positively charged beams with a negatively charged low-energy electron beam, in a device usually referred to as an electron lens. Doing so avoids the coherent instabilities seen in DCI, as the electron beam will not couple back to the hadron beam, except for single-pass effects; these can be significant [13, 14] and may require the addition of a transverse damper in RHIC. Two electron lenses were installed in the Tevatron [8, 13, 15–19], where they were routinely used as a gap cleaner, but not for head-on beam–beam compensation. The Tevatron experience is valuable for several reasons: (i) the reliability of the technology was demonstrated, as no store was ever lost because of the lenses [20]; (ii) the tune shift of selected bunches due to PACMAN effects was corrected, leading to lifetime improvements [16]; (iii) the sensitivity to positioning errors, transverse profile shape, and electron beam current fluctuations was explored [21]; (iv) experiments with a Gaussian profile electron beam were performed; and (v) a hollow electron beam was tested in a collimation scheme [19]. For the design of the RHIC electron lenses we have benefited greatly from the Tevatron experience. We have also drawn on the expertise gained in the construction and operation of an Electron Beam Ion Source (EBIS) at Brookhaven National Laboratory (BNL) [22, 23], which is a device similar to an electron lens but with a different purpose.

In RHIC there are two head-on beam–beam interactions at interaction points IP6 and IP8 (Fig. 1), as well as four long-range beam–beam interactions with large separation (about 10 mm) between the beams at the other interaction points. The luminosity is limited by the head-on effect in polarized proton operation [24–30], as can be seen in Fig. 2. Bunches with two collisions experience a larger proton loss throughout the store than bunches with only one collision. The enhanced loss is particularly strong at the beginning of a store. Beam–beam effects in other hadron colliders are reported in Refs. [31–36].

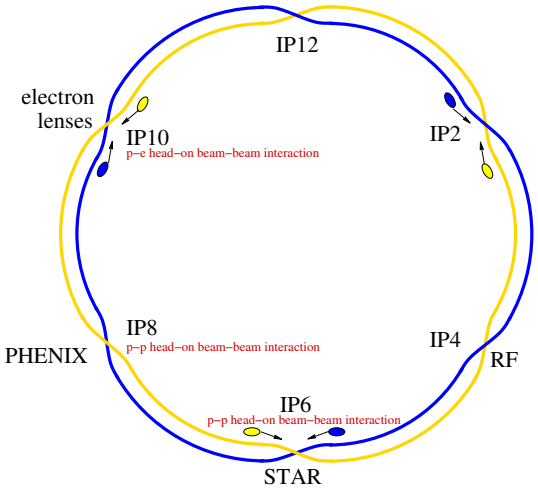

Figure 1: General layout of RHIC with locations of the head-on beam–beam interactions and electron lenses.

We consider the partial indirect compensation of the head-on beam–beam effect with one electron lens in each ring. Together with intensity and emittance upgrades [37], our goal is to approximately double the luminosity over what can be achieved without these upgrades.

This article gives a summary of previous studies and progress reports on head-on beam–beam compensation in RHIC with electron lenses [38–74], updated with the latest available information.

* Work supported by Brookhaven Science Associates LLC under Contract no. DE-AC02-98CH10886 with the U.S. Department of Energy.

† Wolfram.Fischer@bnl.gov

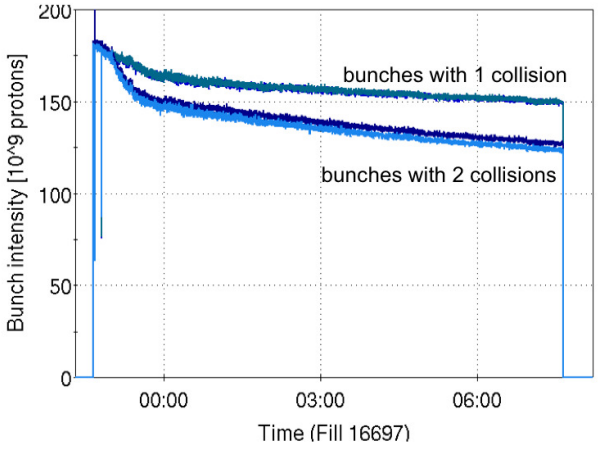

Figure 2: Time-dependent intensity of polarized proton bunches with one or two head-on collisions during the 2012 run.

HEAD-ON BEAM–BEAM COMPENSATION

If a collision of a proton beam with another proton beam is followed by a collision with an electron beam, the head-on beam–beam kick can in principle be reversed. For simplicity we consider only the horizontal plane and beams with a Gaussian transverse distribution. Figure 3 shows the beam line layout for head-on compensation, and Fig. 4 shows the normalized phase space view.

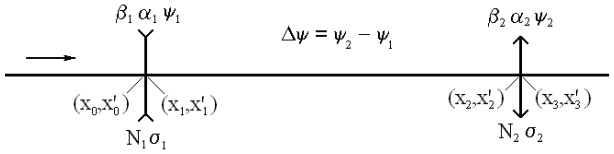

Figure 3: Schematic of head-on beam–beam compensation in a beam line view. At the first location, with lattice parameters $(\beta_1, \alpha_1, \psi_1)$, a proton experiences a beam–beam kick from another proton bunch with intensity N_1 and root-mean-square beam size σ_1. At the second location, with lattice parameters $(\beta_2, \alpha_2, \psi_2)$, another beam–beam kick is generated by the electron beam with effective bunch intensity N_2 and root-mean-square beam size σ_2.

Before experiencing a beam–beam kick from another proton beam at location 1, a proton has transverse phase space coordinates (x_0, x_0'). The proton then receives a kick from the other proton beam [75],

$$\Delta x_0' = \frac{2N_1 r_0}{\gamma x_0}\left[1 - \exp\left(-\frac{x_0^2}{2\sigma_1^2}\right)\right],$$

where N_1 is the bunch intensity of the second proton beam, γ is the relativistic factor of the proton receiving the kick, r_0 is the classical proton radius, and σ_1 is the root-mean-square (rms) beam size of the second proton beam. The

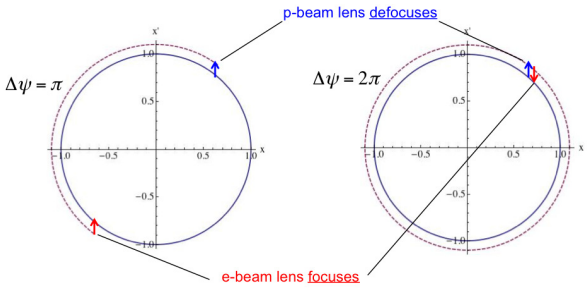

Figure 4: Schematic of head-on beam–beam compensation in a normalized phase space view.

new coordinates are then

$$x_1 = x_0,$$
$$x_1' = x_0' + \Delta x_0'.$$

After transport through the linear beam line, the coordinates are

$$x_2 = M_{11}x_1 + M_{12}x_1',$$
$$x_2' = M_{21}x_1 + M_{22}x_1',$$

with (see [76, 77])

$$M_{11} = \sqrt{\frac{\beta_2}{\beta_1}}(\cos\Delta\psi + \alpha_1 \sin\Delta\psi),$$
$$M_{12} = \sqrt{\beta_1\beta_2}\,\sin\Delta\psi,$$
$$M_{21} = -\frac{1+\alpha_1\alpha_2}{\sqrt{\beta_1\beta_2}}\sin\Delta\psi + \frac{\alpha_1-\alpha_2}{\sqrt{\beta_1\beta_2}}\cos\Delta\psi,$$
$$M_{22} = \sqrt{\frac{\beta_1}{\beta_2}}(\cos\Delta\psi - \alpha_2\sin\Delta\psi)$$

where $\Delta\psi = \psi_2 - \psi_1$. In the electron lens, the proton receives the kick

$$\Delta x_2' = -\frac{2N_2 r_0}{\gamma x_2}\left[1 - \exp\left(-\frac{x_2^2}{2\sigma_2^2}\right)\right],$$

where N_2 is the effective bunch intensity of the electron lens beam (i.e. the number of electrons the proton passes in the lens) and σ_2 is the rms beam size of the electron lens beam. The coordinates after passing the electron lens are then

$$x_3 = x_2,$$
$$x_3' = x_2' + \Delta x_2'.$$

One can now express the final coordinates (x_3, x_3') as a function of the intensities (N_1, N_2) and require, for exact compensation, that

$$x_3(N_1, N_2) = x_3(0, 0) \quad (1)$$

and

$$x_3'(N_1, N_2) = x_3'(0, 0), \quad (2)$$

i.e. that the final coordinates are the same with and without beam–beam interaction and compensation. From the condition (1) it follows that $M_{12} = 0$ and hence $\Delta\psi = k \cdot \pi$, where k is an integer. From the condition (2) it follows that $N_1 = N_2$ and $\sigma_1^2/\sigma_2^2 = \beta_1/\beta_2$.

Therefore, if the following three conditions are met, the beam–beam kicks are cancelled exactly.

1. The ion beam and electron beam produce the same amplitude-dependent force by having the same effective charge and profile.
2. The phase advance between the two beam–beam collisions is a multiple of π in both transverse planes.
3. There are no nonlinearities between the two collisions.

In practice the above can be achieved only approximately. Deviations from condition 1 include:

- an electron current that does not match the proton bunch intensity;
- a non-Gaussian electron beam profile (assuming that the proton beam transverse profile is Gaussian);
- an electron beam size that differs from the proton beam size;
- time-dependence of the electron and proton beam parameters.

Deviations from condition 2 include:

- a phase advance $\Delta\psi \neq k\pi$ between the head-on collision and the electron lens;
- long bunches, i.e. $\sigma_\mathrm{s} \gtrapprox \beta^*$.

Deviations from condition 3 include:

- lattice sextupoles and octupoles, as well as multipole error between the head-on collision and the electron lens.

Tolerances were studied extensively in simulations and reported in Ref. [70], and bunch length effects have been investigated in Refs. [47, 48]. The Tevatron experience also provides tolerances for positioning errors, transverse shape and size mismatches, and electron current variations. We give the tolerances for all devices below.

We plan to compensate for only one of the two head-on collisions in RHIC, since a full compensation would lead to a small tune spread and could give rise to instabilities.

RHIC ELECTRON LENS DESIGN

In designing the electron lens, we were aiming for a technically feasible implementation that would come as close as possible to the ideal compensation scheme outlined above. In addition, a major design consideration was ease of commissioning and operation. Our goal is a commissioning that is largely parasitic to the RHIC operation for physics. The main design process can be summarized as follows.

Condition 1 (same amplitude-dependent forces from the proton beam and electron lens) has a number of implications. Since both proton beams are round in the beam–beam interactions ($\beta_x^* = \beta_y^*$ and $\epsilon_x = \epsilon_y = \epsilon_n$), we also require that $\beta_x = \beta_y$ at the electron lens location, and require matched transverse proton and electron beam profiles, i.e. that the electron beam profile is also Gaussian with $\sigma_{\mathrm{p},x} = \sigma_{\mathrm{e},x} = \sigma$ and $\sigma_{\mathrm{p},y} = \sigma_{\mathrm{e},y} = \sigma$. The condition $\beta_x = \beta_y$ limits the electron lens locations to the space between the DX magnets; in these locations the RHIC lattice also has a small dispersion.

Table 1: Reference cases for RHIC beam–beam and beam-lens interactions. Bunch intensities without electron lenses are expected to saturate at about 2×10^{11} because of head-on beam–beam effects [30, 70].

Quantity	Unit	Value		
Proton beam parameters				
Total energy E_p	GeV	100	255	255
Bunch intensity N_p	10^{11}	2.5	2.5	3.0
$\beta^*_{x,y}$ at IP6, IP8 (p–p)	m	0.85	0.5	0.5
$\beta^*_{x,y}$ at IP10 (p–e)	m	10.0	10.0	10.0
Lattice tunes (Q_x, Q_y)	–	— (0.695, 0.685) —		
rms emittance ϵ_n, initial	mm mrad	— 2.5 —		
rms beam size at IP6, IP8 σ^*_p	μm	140	70	70
rms beam size at IP10 σ^*_p	μm	485	310	310
rms bunch length σ_s	m	0.50	0.40	0.20
Hourglass factor F, initial	–	0.88	0.85	0.93
Beam–beam parameter ξ/IP	–	0.012	0.012	0.015
Number of beam–beam IPs	–	— 2 + 1[a] —		
Electron lens parameters				
Distance of centre from IP	m	— 2.0 —		
Effective length L_e	m	— 2.1 —		
Kinetic energy E_e	keV	7.8	7.8	9.3
Relativistic factor β_e	–	0.18	0.18	0.19
Electron line density n_e	10^{11} m^{-1}	1.0	1.0	1.2
Electrons in lens N_e1	10^{11}	2.1	2.1	2.5
Electrons encountered N_e2	10^{11}	2.5	2.5	3.0
Current I_e	A	0.85	0.85	1.10

[a] One head-on collision in IP6 and IP8 each, plus a compensating head-on collision in IP10.

The tolerances for the main solenoid field straightness and for the relative beam alignment are easier to meet with a larger proton beam. A larger beam is also less susceptible to coherent instabilities [13, 71]. The β-function at IP10 cannot be larger than 10 m at 250 GeV proton energy without modifications to the buses and feedthroughs of the IR10 superconducting magnets. Such modifications are currently not under consideration because of costs, but could be implemented if coherent instabilities occur and cannot be mitigated by other means.

With a fully magnetized electron beam, the beam size σ_e in the main solenoid is given by its size at the cathode, σ_ec, together with the solenoid fields B_sc at the cathode and B_s in the main solenoid as $\sigma_\mathrm{e} = \sigma_\mathrm{ec}\sqrt{B_\mathrm{sc}/B_\mathrm{s}}$. For technological and cost reasons, the field B_s cannot be much larger than 6 T, and a strong field makes a correction of the field straightness more difficult. The field B_sc has to be large enough to suppress space charge effects. With the limits in the B_sc and B_s fields and a given beam size σ_e, the electron beam size and current density at the cathode follow, and they must be technically feasible. Unlike the Tevatron elec-

tron lenses, we use a DC electron beam to avoid the noise possibly introduced through the high-voltage switches. A DC beam requires the removal of ions created in the electron lens through residual gas ionization.

Condition 2 (phase advance of multiples of π between p–p and p–e interaction) can be achieved through lattice modifications. We have installed four phase-shifter power supplies for both transverse planes of both rings so that the betatron phase between IP8 and the electron lenses in IR10 can be adjusted. To have $\Delta\psi = k\pi$ in both planes of both rings, it is also necessary to change the integer tunes from $(28, 29)$ to $(27, 29)$ in the Blue ring and from $(28, 29)$ to $(29, 30)$ in the Yellow ring to find a solution. With the new lattices, higher luminosities were reached in 2013 than in previous years, but the polarization was lower. The lower polarization is still being investigated and may not have resulted from the new lattices. Other lattice options are also under study: (i) a solution was found for the Yellow ring that maintains the integer tunes of $(28, 29)$ and has the correct phase advances; (ii) the phase advance of a multiple of π may also be realized between IP6 and the electron lenses.

Condition 3 (no nonlinearities between the p–p and p–e interactions) is best achieved when the p–e interaction is as close as possible to the p–p interaction. With the location in IR10 (Fig. 1), there is only one arc between the p–p interaction at IP8 and the p–e interaction at IR10. In this configuration, a proton, after receiving a beam–beam kick at IP8, passes a triplet with nonlinear magnetic fields from field errors, an arc with chromaticity sextupoles and dodecapoles in the quadrupoles as dominating nonlinear field errors, and another triplet in IR10. To avoid bunch length effects, the parameter β^* cannot be too small [47, 48]. In simulations, a value as low as $\beta^* = 0.5$ m was found to be acceptable [70].

The location of both the Blue and the Yellow electron lenses in IR10, in a section common to both beams (Fig. 5), allows local compensation of the main solenoid effect on both linear coupling and spin orientation by having the two main solenoids with opposing field orientations. At 255 GeV proton energy, one superconducting solenoid with a 6 T field introduces coupling that leads to $\Delta Q_{\min} = 0.0023$ [51] and increases all spin resonance strengths by 0.003 [78]. In this configuration it is also possible to ramp the magnets together during RHIC stores without affecting the beam lifetime or spin orientation.

The instrumentation must allow for monitoring of the electron beam current and shape as well as the relative position and angle of the electron and proton beams in the electron lens. Two modes are foreseen: a setup mode in which the electron beam current is modulated and affects only a single bunch in RHIC, and a compensation mode with a DC electron beam. The main parameters of the electron beams are presented in Table 1.

A RHIC electron lens consists of (see Fig. 6) an electron gun, an electron beam transport to the main solenoid, the superconducting main solenoid in which the interaction with the hadron beam occurs, an electron beam transport to the collector, an electron collector, and instrumentation.

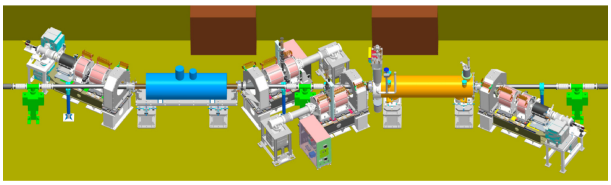

Figure 5: Layout of the two electron lenses in IR10. In 2013 the Blue lens (left) had the EBIS spare solenoid installed instead of the superconducting solenoid designed for the electron lens. In each lens three beams are present, the two proton beams and the electron beam acting on one of the proton beams; the proton beams are vertically separated.

Electron Gun

The electron gun (see Fig. 7 and Table 2) [59] has to provide a beam with a transverse profile that is close to Gaussian. Considering the magnetic compression of the electron beam into the main solenoid centre with a maximum magnetic field of 6.0 T, a cathode radius of 4.1 mm gives a Gaussian profile with 2.8 rms beam sizes. The perveance of the gun is $P_{\rm gun} = 1.0 \times 10^{-6}$ AV$^{-1.5}$. The current density of the electron beam on its radial periphery can be changed with the control electrode voltage (Fig. 7, top), while the general shape of the beam profile remains Gaussian. The cathodes (LB_6 and IrCe) were produced at BINP in Novosibirsk [79]. With a nominal current density of 12 A/cm^2, IrCe was chosen as the cathode material for its long lifetime (greater than 10 000 h).

An assembled gun is shown in the bottom panel of Fig. 7. The gun has three operating modes: (i) DC for continuous compensation; (ii) 100 Hz for electron beam positioning with BPMs, such that the electron current rises between the last two RHIC bunches and falls in the abort gap; (iii) 78 kHz for single-bunch compensation, with rise and fall time as in the 100 Hz mode.

The gun and collector vacuum is UHV compatible, with a design pressure of 10^{-10} Torr and a nominal pressure of 10^{-11} Torr for the interface to the RHIC warm bore. For this reason, all of the components are bakeable to 250°C. The gun and collector chambers will have a confined gas load by using a conductance-limiting aperture and enough installed pumping speed. All vacuum chambers interfacing with the RHIC warm bore will be made from stainless steel.

Electron Collector

The collector spreads the electrons on the inside of a cylindrical surface that is water-cooled on the outside (see Fig. 8). Simulations give a power density of 10 W/cm^2 for a 10 A electron beam, decelerated to 4 keV. The collector can absorb up to four times this power density [59]. The design is dictated primarily by the UHV requirements of RHIC. It separates the heavily bombarded area from the rest of

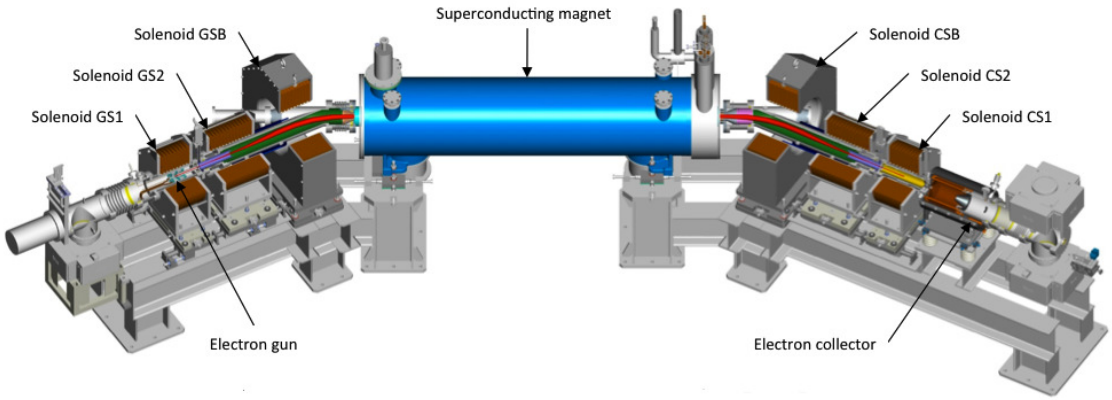

Figure 6: RHIC electron lens. The electrons in the DC beam move from left to right and interact with the protons, which move in the opposite direction, inside the superconducting solenoid.

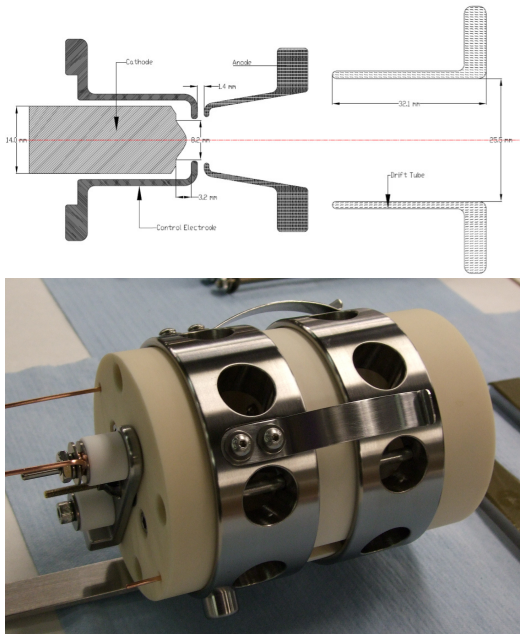

Figure 7: Gun schematic (top) and manufactured gun (bottom).

the electron lens by using a small diaphragm. A magnetic shield leads to fast diverting electrons inside the collector. The reflector has a potential lower than the cathode and pushes electrons outwards to the water-cooled cylindrical surface. Under a load twice as high as expected from a 2 A electron beam, the maximum temperature on the inner surface of the shell is 102°C. This temperature is acceptable for the material (copper) and for UHV conditions in RHIC. Twenty tubes with an ID = 8.0 mm are brazed to the outside of the cylindrical shell and are connected in parallel for water flow (Fig. 8).

The collector design also limits the flow of secondary and backscattered electrons from the collector towards the interaction region because the volume is magnetically shielded.

Table 2: Main parameters of the thermionic electron gun.

Quantity	Unit	Value
Perveance	μA V$^{-3/2}$	1.0
Voltage	kV	10
Current	A	1.0
Profile	–	Gaussian
Cathode radius	mm / σ	4.1 / 2.8
Max B-field	T	0.8
Modes	–	DC, 100 Hz, 78 kHz

The gun and collector power supplies are referenced to the cathode. The gun supplies include the cathode bias supply, the cathode heater, the beam-forming supply, and two anode supplies (DC and pulsed). The collector power supply is rated with 10 kV at 2 A, and will limit the energy deposited in the device should an arc occur. An ion reflector is powered with respect to the cathode potential. A suppressor element is powered with respect to the collector.

Superconducting Main Solenoid

A superconducting solenoid guides and stabilizes the low-energy electron beam during the interaction with the proton beam, and allows for magnetic compression of the electron beam size to the proton beam size. The superconducting main solenoid is a warm bore magnet with an operating field of 1–6 T (Fig. 9). The cryostat includes a number of additional magnets for a total of 17 [62]. The main parameters are given in Table 3.

Fringe field (FF) solenoid coils at both ends are included to allow for a guiding and focusing solenoid field for the electrons of no less than 0.3 T between the superconducting magnet and the warm transport solenoids GSB and CSB (see Fig. 6). To achieve the desired field uniformity over a range of field strengths B_s, anti-fringe field (AFF) coils are placed next to the FF coils. The FF and AFF coils on

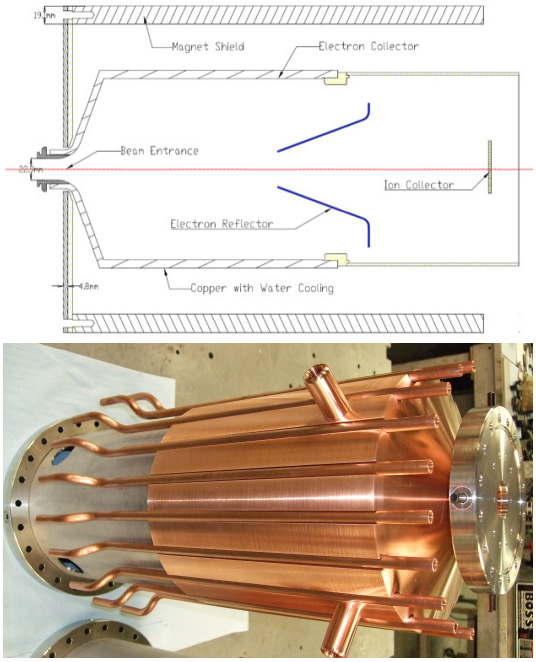

Figure 8: Collector schematic (top) and collector during manufacturing (bottom).

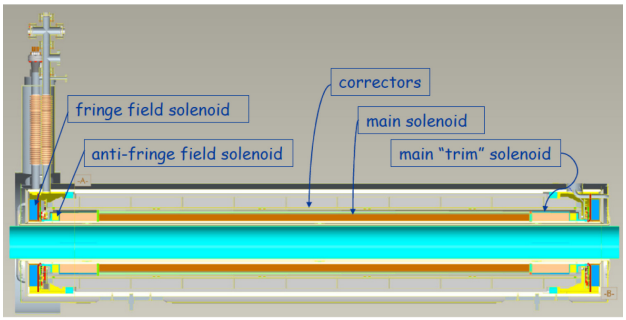

Figure 9: Superconducting main solenoid with fringe and anti-fringe solenoids, and straightness and angle correctors.

both ends can be powered independently to avoid forming a magnetic bottle with a low main field B_s, which would trap backscattered electrons. Extraction of scattered electrons is also possible by using a split electrode [69].

Included in the cryostat are five short (0.5 m) dipole correctors in both the horizontal and the vertical planes, to correct the solenoid field straightness to ± 50 μm. A long (2.5 m) dipole corrector in each transverse plane allows the angle of the electron beam inside the main magnet to be changed by ± 1 mrad (at 6 T) to align the electron and proton beams.

To reduce the number of layers in the main, FF, and AFF coils, and thereby the manufacturing time, a relatively large conductor was chosen, and the current in these coils was 430 A, 470 A, and 330 A, respectively [62]. A total of 17 individual coils (main coil, two FF coils, two AFF coils, ten straightness dipole correctors, and two angle dipole correctors) can be powered.

Table 3: Main parameters of the superconducting solenoids and corrector magnets in the same cryostat.

Quantity	Unit	Value
Cryostat length	mm	2838
Coil length	mm	2360
Warm bore inner diameter	mm	154
Uniform field region	mm	± 1050
Main coil layers	–	22 (11 double)
Additional trim layers in ends	–	4 (2 double)
Wire I_c specification (4.2 K, 7 T)	A	> 700
Operating main field B_s	T	1–6
Field uniformity $\Delta B_s/B_s$	–	± 0.006 (1–6 T)
Field straightness, after correction	μm	± 50 (1–6 T)
Straightness correctors (5H + 5V)	T m	± 0.010
Angle correctors (1H + 1V)	T m	± 0.015
Inductance	H	14
Stored energy (6 T)	MJ	1.4
Current (6 T)	A	430 (473[a])

[a] First double layer disabled.

The magnet is bath-cooled at a temperature just above 4.5 K, dictated by the operating pressure of RHIC cryogenic system's main warm return header. The current leads are all conventional vapour-cooled leads with individual flow controllers. The magnet's thermal shield and supports intercepts are cooled by the balance of the boil-off vapour not used by the current leads, which also returns to the main warm return header. The total flow rate draw from the RHIC cryogenic system is 1.6 g/s for each solenoid. Liquid helium can be supplied from a local Dewar when the RHIC refrigerator is not running.

Both magnets were tested vertically and reached 6.6 T, 10% above the maximum operating field, after a few training quenches. The magnets are now fully cryostatted. During the vertical test of the first magnet, a short in the first layer was detected, and the first double layer was grounded permanently. This required raising the operating current from 440 A to 473 A.

The field measurement system is under development. With proton rms beam sizes as small as 310 μm in the electron lenses, a deviation by no more than 50 μm of the solenoid field lines from straight lines is targeted. A needle-and-mirror system has been constructed that can be used in the RHIC tunnel to both measure the straightness of the field lines and verify the correction with the integrated short dipole correctors. The needle-and-mirror measurement system is being cross-checked with a vibrating wire system [80] using the second superconducting solenoid.

Warm Magnets

The electron beam is transported from the gun to the main solenoid and from the main solenoid to the collector through three warm solenoids each (Fig. 6) [54, 59]. These provide focusing with a solenoid field of at least 0.3 T along the whole transport channel. Within the GS2 and CS2 solenoids are also horizontal and vertical steering

magnets that can move the beam by ±5 mm in the main solenoid in either plane.

The solenoids are made of pancake coils whose field errors have been optimized [56]. The power consumption of both electron lenses with nominal parameters is limited to a total of 500 kW to avoid upgrades to the electrical and cooling water infrastructure in IR10. The main parameters are given in Table 4. All warm magnets and associated power supplies are installed (Fig. 10).

Table 4: Main parameters of the warm magnets.

Quantity	Unit	GS1 CS1	GS2 CS2	GSB CSB	GSX CSX	GSY CSY
ID	mm	174	234	480	194	210
OD	mm	553	526	860	208	224
Length	mm	262	379	262	500	500
No. layers	–	13	10	13	12	12
No. pancakes	–	9	13	9		
Inductance	mH	20	20	40	0.2	0.2
Resistance	mΩ	40	50	80	20	20
Current	A	1188	731	769	258	271
Power	kW	58	26	45	1.4	1.7
ΔT	K	13.4	3.6	14.2	5.9	6.9
Δp	bar	1.5	1.5	1.5	1.5	1.5
Solenoid field B_s	T	0.8	0.45	0.32		

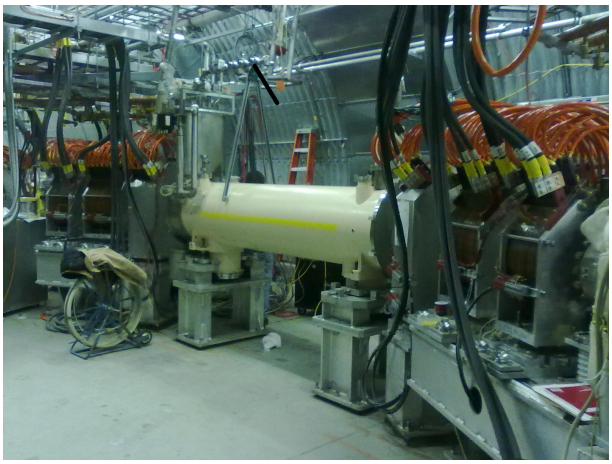

Figure 10: Yellow electron lens as installed in 2013. Visible are the gun side (left), the superconducting main solenoid (centre), and the collector side (right).

Instruments and Vacuum System

The instrumentation monitors the current and shape of the electron beam, the electron beam losses, and the overlap of the electron beam with the proton beam. The following items are included (the quantities given in parentheses are for each lens):

- dual-plane beam position monitors (2);
- e–p beam overlap monitor based on backscattered electrons (1) [65];
- differential current monitor (1);
- beam loss monitor drift tubes (8);
- collector temperature sensor (1);
- profile monitor (YAG screen) (1);
- profile monitor (pin-hole) (1);
- ion collector (1).

The layout of the vacuum system with the drift tubes is shown in Fig. 11. A total of eight drift tubes allow for changes in the electron beam energy and the removal of ions in the interaction region; the split drift tube 4 enables the removal of backscattered electrons [69], which can be trapped with a low main field B_s and high fringe fields. Figure 12 shows the detail of a section containing a beam position monitor (BPM), two drift tubes, cables, feedthroughs, and a heat sink to cool the cables, which can heat up when the proton beam deposits radio-frequency energy in the structure.

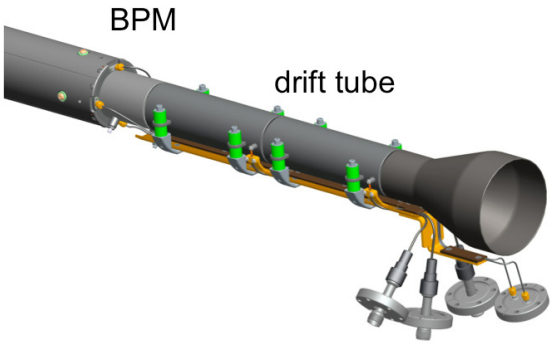

Figure 12: Beam position monitor and drift tubes with high-voltage stand-offs and cable.

The BPMs see only a signal with a pulsed beam. The proton beams are bunched, and a fill pattern can be created so that a bunch in one beam is detected when there is a gap in the other beam. The electron beam needs to be pulsed (at 100 Hz or 80 kHz) to be visible. The BPMs are used to bring the electron and proton beams in close proximity. The final alignment is done with the beam overlap monitor based on backscattered electrons [65]. Alignment was found to be a critical parameter in the Tevatron electron lenses, and the beams have to be aligned to within a fraction of the rms beam size, which can be as small as 310 μm (see Table 1). Figure 13 shows the beam overlap monitor.

The differential current monitor, drift tubes, ion collector, and collector temperature sensor all monitor the electron beam loss in the lens. The YAG screen and pin-hole profile monitors can only be used in a low-power mode. The extracted ion current is monitored in a collector [59].

TEST BENCH RESULTS

The test bench (Figs. 15 and 16) uses the location and the superconducting solenoid of the BNL EBIS test stand. Of the RHIC electron lenses, the following components were installed: a gun and collector, a GS1 solenoid with power supply, a movable pin-hole detector, a movable YAG screen with camera, and an electron halo detector.

The test bench work is complete and the following have been demonstrated [68, 72–74].

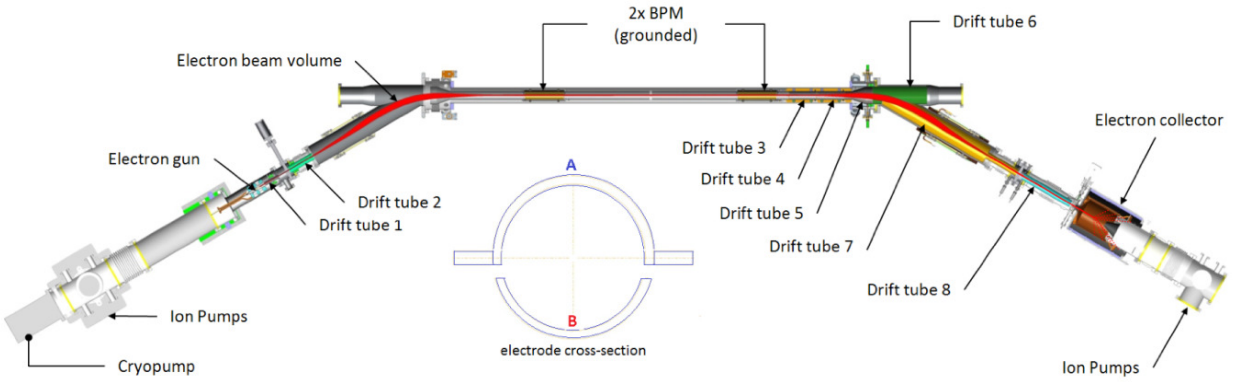

Figure 11: Layout of the drift tube system. The inset shows the cross-section of drift tube 4, which is split for the removal of trapped electrons [69].

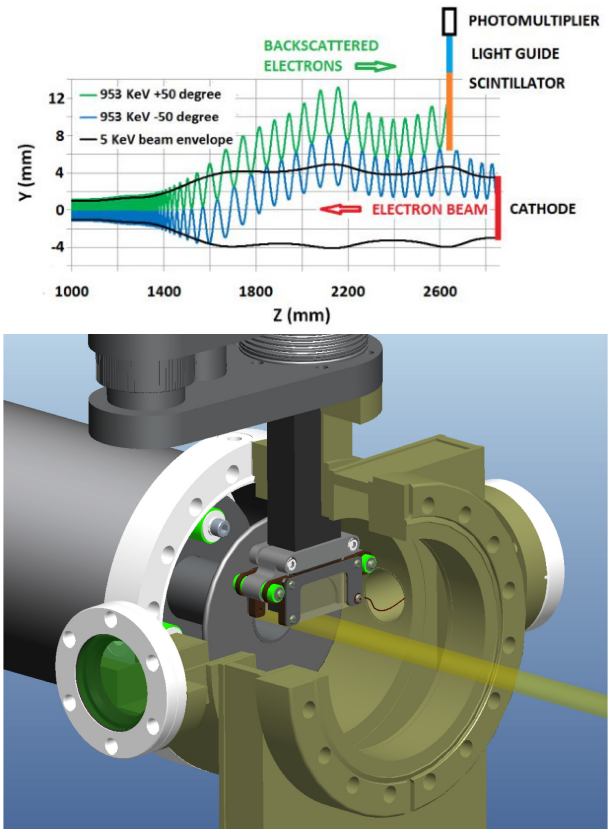

Figure 13: Beam overlap monitor using backscattered electrons [65]. The top view is a schematic showing two trajectories of backscattered electrons arriving at the gun above the primary electron beam; the bottom view shows the positioning mechanism of the detector.

- The gun operated in 80 kHz pulsed mode and DC mode, and reached 1 A of DC current with a current ripple of $\Delta I/I = 0.075\%$.
- The gun perveance with a La_6B cathode was measured to be 0.93 $\mu AV^{-3/2}$.
- The collector temperature and pressure was measured with the 1 A DC current and found to be within expectations.
- The Gaussian transverse electron beam profile was verified.
- The machine protection system was prototyped.
- Part of the controls software was tested.

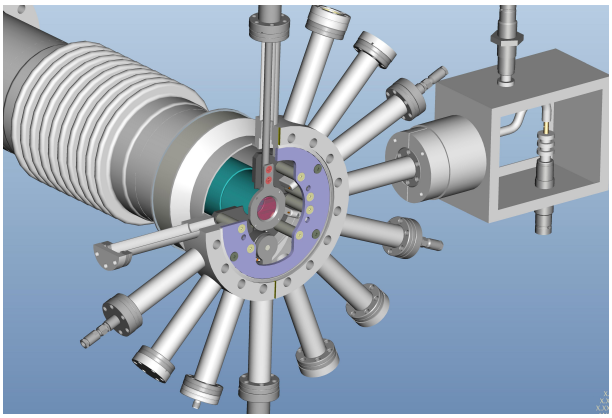

Figure 14: Instrument holder in front of the collector. Visible are the halo detector, YAG screen (inserted), and pinhole detector (retracted).

After completion of the test bench, the components were removed and installed in the RHIC tunnel and service building.

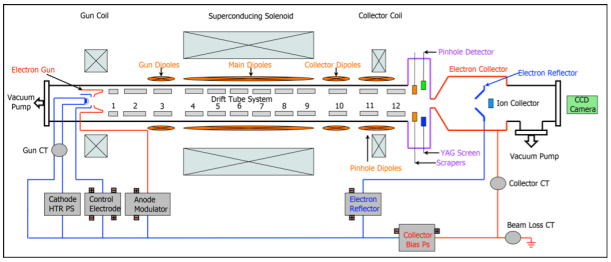

Figure 15: Schematic of the electron lens test bench layout.

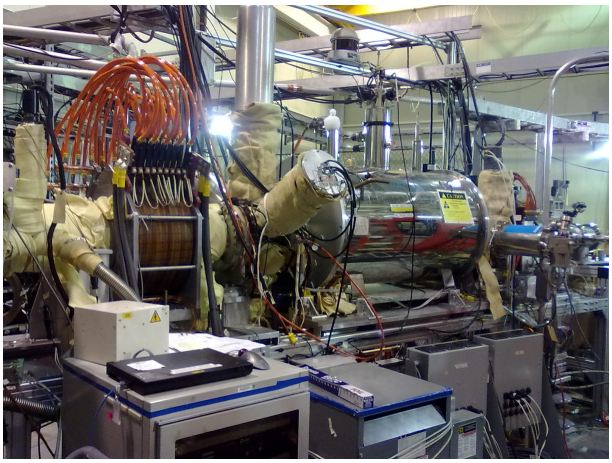

Figure 16: RHIC electron lens test bench. The electron beam travels from left to right, and GS1 is visible.

STATUS AND OUTLOOK

For the ongoing RHIC Run-13, the hardware of both lenses is partially installed (Fig. 5). The Blue lens has a complete electron beam transport system, although instead of the superconducting main solenoid designed for the electron lens a spare solenoid of the BNL EBIS is installed. This magnet is a 2 m-long superconducting solenoid with a maximum field strength of 5 T, but it does not have an iron yoke and therefore the field lines are not straight enough for beam–beam compensation; it does, however, allow for propagation of the electrons from the gun to the collector even at field strengths as low as 1 T. The low field is necessary to minimize the effect on the proton spin, as long as the second superconducting solenoid is not yet powered. The Blue lens also has a full complement of instrumentation, with the exception of the overlap monitor based on backscattered electrons. All drift tubes are grounded. In this configuration, all warm magnets can be commissioned as well as the electron beam in pulsed mode. The two dual-plane BPMs inside the superconducting solenoid, the YAG screen profile monitor, and the pin-hole detector can be tested. Interaction with the proton beam is in principle possible.

The Yellow lens has one of the new superconducting solenoids installed, but with a straight beam pipe that does not have BPMs or drift tubes (i.e. the vacuum system of the electron gun and collector is not connected to the proton beam vacuum system). This configuration allows for commissioning of the superconducting main solenoid and all superconducting correctors, as well as all warm magnets. The Yellow lens is shown in Fig. 10.

The second superconducting solenoid is set up in the Superconducting Magnet Division as a test bed for the field-straightness measurement system. As of the submission of this paper, the following have been achieved. A new lattice was commissioned for both rings that has a phase advance of a multiple of π between IP8 and the electron lens; for this new phase shifter, power supplies were installed in both rings and both transverse planes. A bunch-by-bunch loss monitor has become available, and bunch-by-bunch BTF measurements are being tested. The derivation of the incoherent beam–beam tune spread in the presence of coherent modes from transverse BTF measurements is under investigation [81]. In the Blue lens, a field of 1 T in the superconducting solenoid has been established. All warm solenoids were tested at operating currents, and all GSB and CSB solenoids ran concurrently with RHIC polarized proton operation.

In the summer of 2013 the second superconducting main solenoid will be installed, and the field straightness of both magnets will be measured in place and corrected. After that, the installation will be completed for both lenses, including the overlap detector based on backscattered electrons.

In 2014 RHIC is likely to operate predominantly with heavy ions. The beam–beam effect with heavy ions is too small for compensation, but all electron beam operating modes (pulsed and DC) can be established, and the electron beam can interact with the ion beam. The first compensation test can be done in polarized proton operation.

SUMMARY

Partial head-on beam–beam compensation is being implemented in RHIC. One of two beam–beam interactions is to be compensated with two electron lenses, one for each of the two proton beams. This allows for an increase in the bunch intensity with a new polarized proton source [37], with the goal of doubling the average luminosity in polarized proton operation.

The components of two electron lenses have been manufactured and partially installed. The current installation allows for commissioning of the warm magnets, electron beam, and instrumentation in the Blue lens. In the Yellow lens, the new superconducting solenoid and the warm magnets can be commissioned. First tests with ion beams are anticipated for the next year, after which the compensation can be commissioned for polarized proton operation.

ACKNOWLEDGMENTS

We are grateful to V. Shiltsev, A. Valishev, and G. Stancari of FNAL for many discussions on the Tevatron electron lenses and for the opportunities to participate in electron lens studies at the Tevatron. We also greatly benefited from the experience of the BNL EBIS team, including J. Alessi, E. Beebe, M. Okamura, and D. Raparia. We had many fruitful conversations about beam–beam and compensation problems with V. Shiltsev, A. Valishev, T. Sen, and G. Stancari of FNAL; X. Buffat, R. DeMaria, U. Dorda, W. Herr, J.-P. Koutchouk, T. Pieloni, F. Schmidt, and F. Zimmerman of CERN; K. Ohmi of KEK; V. Kamerdziev of FZ Jülich; A. Kabel of SLAC; and P. Görgen of TU Darmstadt. We are thankful to the U.S. LHC Accelerator Research Program (LARP) for support of beam–beam simulations. We also acknowledge the technical and administrative support received from the BNL Su-

perconducting Magnet Division, as well as from all groups of the Collider-Accelerator Department, in particular K. Mirabella and G. Ganetis.

REFERENCES

[1] G. Arzelia et al., Proc. 8th Int. Conf. High Energy Acc., p. 150 (1971).

[2] M. Bergher et al., "Status Report on D.C.I.," Proc. 1979 Particle Accelerator Conf., San Francisco, Calif., USA, pp. 3559–3561 (1979).

[3] Ya.S. Derbenev, "Collective Instability of Compensated Colliding Beams," Nuclear Physics Institute, Siberian Division, Academy of Sciences USSR, Novosibirsk, Report IYAF 70-72, in Russian (1972); SLAC-TRANS 151 in English.

[4] N.N. Chau and D. Potau, "Stabilité des oscillations transverse dans un anneau à charge d'espace compensée," LAL Orsay (1974 and 1975).

[5] B. Podobedov and R.H. Siemann, "Coherent Beam–Beam Interaction with Four Colliding Beams," Phys. Rev. E 52 (1995) 3066.

[6] E. Tsyganov, R. Meinke, W. Nexsen, and A. Zinchenko, "Compensation of the Beam–Beam Effect in Proton Colliders," SSCL-PREPRINT-519 (1993).

[7] E. Tsyganov, E. Tarantin, and A. Zinchenko, "Compensation of Space Charge Effect at Beam–Beam Interactions in Proton Proton Colliders," JINR-E9-96-4 (1996).

[8] V. Shiltsev, V. Danilov, D. Finley, and A. Sery, "Considerations on Compensation of Beam–Beam effects in the Tevatron with Electron Beams," Phys. Rev. ST Accel. Beams 2 (1999) 071001.

[9] E.N. Tsyganov, A. Taratin, and A.I. Zinchenko, "Beam–Beam Compensation at the LHC," CERN SL-Note-95-116-AP (1995).

[10] W. Scandale and F. Zimmermann, "Head-on Compensation in LHC," presentation at US LARP Mini-Workshop on Beam-Beam Compensation, SLAC (2009).

[11] U. Dorda, F. Zimmermann, W. Fischer, and V. Shiltsev, "LHC Beam–Beam Compensation Using Wires and Electron Lenses," Proc. 2007 Particle Accelerator Conf., Albuquerque, New Mexico, USA; LHC-PROJECT-Report-1023 (2007).

[12] Y. Ohnishi and K. Ohmi, "Beam–Beam Simulations in Four-Beam Scheme for High-Luminosity e+e- Collider," Proc. HALO'03 and Beam-Beam'03, Montauk, New York, AIP Conference Proceedings 693 (2003).

[13] A. Burov, V. Danilov, and V. Shiltsev, "Transverse Beam Stability with an Electron Lens," Phys. Rev. E 59 (1999) 3605.

[14] S. White, M. Blaskiewicz, and W. Fischer, "Coherent Beam–Beam Effects in Experiments and Implications for Head-on Beam–Beam Compensation," these proceedings.

[15] V. Shiltsev and A. Zinchenko, "Electron Beam Distortions in Beam–Beam Compensation Setup," Phys. Rev. ST Accel. Beams 1 (1998) 064001.

[16] V. Shiltsev, Y. Alexahin, K. Bishofberger, V. Kamerdzhiev, G. Kuznetsov, and X.-L. Zhang, "Experimental Demonstration of Colliding-Beam-Lifetime Improvement by Electron Lenses," Phys. Rev. Lett. 99 (2007) 244801.

[17] X.-L. Zhang, K. Bishofberger, V. Kamerdzhiev, V. Lebedev, V. Shiltsev, R. Thurman-Keup, and A. Tollestrup, "Generation and Diagnostics of Uncaptured Beam in the Fermilab Tevatron and its Control by Electron Lenses," Phys. Rev. ST Accel. Beams 11 (2008) 051002.

[18] V. Shiltsev et al., "Tevatron Electron Lenses: Design and Operation," Phys. Rev. ST Accel. Beams 11 (2008) 103501.

[19] G. Stancari, A. Valishev, G. Annala, G. Kuznetsov, V. Shiltsev, D. A. Still, and L. G. Vorobiev, "Collimation with Hollow Electron Beams," Phys. Rev. Lett. 107 (2011) 084802.

[20] V. Shiltsev, private communication.

[21] G. Stancari and A. Valishev, "Beam-Beam Compensation Studies in the Tevatron with Electron Lenses," these proceedings.

[22] J. Alessi (ed.), "Electron Beam Ion Source Pre-Injector Project (EBIS), Conceptual Design Report," BNL-73700-2005-IR (2005).

[23] J.G. Alessi et al., "Commissioning of the EBIS-based Heavy Ion Preinjector at Brookhaven," Proc. LINAC2010, Tsukuba, Japan, pp. 1033–1037 (2010).

[24] C. Montag et al., "RHIC Performance as a 100 GeV Polarized Proton Collider in Run-9," Proc. 2010 Int. Particle Accelerator Conf., Kyoto, Japan, pp. 531–533 (2010).

[25] H. Huang et al., "RHIC Polarized Proton Operation and Highlights," Proc. 2011 Int. Particle Accelerator Conf., San Sebastian, Spain, pp. 1888–1890 (2011).

[26] V. Schoefer et al., "RHIC Polarized Proton Operation in Run 12," Proc. 2012 Int. Particle Accelerator Conf., New Orleans, Louisiana, USA, pp. 184–186 (2012).

[27] Y. Luo, M. Bai, W. Fischer, C. Montag, and S. White, "Beam–Beam Effects in RHIC," BNL C-AD/AP/467 (2012).

[28] Y. Luo, M. Bai, W. Fischer, C. Montag, and S. White, "Beam–Beam Effects in RHIC," Proc. 52th ICFA Advanced Beam Dynamics Workshop on High Intensity High Brightness Hadron Beams (HB2012), Beijing, China (2012).

[29] S.M. White, W. Fischer, and Y. Luo, "Coherent Beam–Beam Effects Observation and Mitigation at the RHIC Collider," Proc. 2012 Int. Particle Accelerator Conf., New Orleans, Louisiana, USA, pp. 193–195 (2012).

[30] Y. Luo and W. Fischer, "Beam–Beam Observations in RHIC," these proceedings.

[31] F. Zimmermann and J. Poole (eds.), Proc. Workshop on Beam-Beam Effects in Large Hadron Colliders, LHC99, CERN, CERN-SL-99-039 AP (1999).

[32] T. Sen and M. Xiao (eds.), Proc. Workshop on Beam–Beam Effects in Circular Colliders, FNAL, FERMILAB-Conf-01/390-T (2001)

[33] W. Fischer and T. Sen (eds.), Proc. HALO'03 and Beam-Beam'03, Montauk, New York, USA, AIP Conference Proceedings 693 (2003).

[34] V. Shiltsev, Y. Alexahin, V. Lebedev, P. Lebrun, R. S. Moore, T. Sen, A. Tollestrup, A. Valishev, and X. L. Zhang, "Beam–Beam Effects in the Tevatron," Phys. Rev. ST Accel. Beams 8 (2005) 101001.

[35] W. Fischer (issue ed.) and W. Chou (exec. ed.), *ICFA Beam Dynamics Newsletter No. 52: Current Beam–Beam Problems* (2010).

[36] W. Herr, E. Metral, and T. Pieloni (eds.), these proceedings.

[37] A. Zelenski, "OPPIS with Fast Atomic Beam Source," presentation at 2011 Particle Accelerator Conf., New York, USA (2011).

[38] Y. Luo and W. Fischer, "Outline of Using an Electron Lens for the RHIC Head-on Beam–Beam Compensation," BNL C-A/AP/286 (2007).

[39] Y. Luo, W. Fischer, and N. Abreu, "Stability of Single Particle Motion with Head-on Beam–Beam Compensation in the RHIC," BNL C-A/AP/310 (2008).

[40] Y. Luo, W. Fischer, N. Abreu, E. Beebe, J. Beebe-Wang, C. Montag, M. Okamura, A. Pikin, and G. Robert-Demolaize, "Head-on Beam–Beam Compensation with Electron Lenses in the Relativistic Heavy Ion Collider," Proc. 2008 European Particle Accelerator Conf., Genoa, Italy, pp. 1616–1618 (2008).

[41] Y. Luo, G. Robert-Demolaize, N. Abreu, and W. Fischer, "Multi-Particle Weak-Strong Simulation of Head-on Beam–Beam Compensation in the RHIC," Proc. 2008 European Particle Accelerator Conf., Genoa, Italy, pp. 3125–3127 (2008).

[42] N.P. Abreu, W. Fischer, Y. Luo, and G. Robert-Demolaize, "The Effect of Head-on Beam–Beam Compensation on the Stochastic Boundaries and Particle Diffusion in RHIC," Proc. 2008 European Particle Accelerator Conf., Genoa, Italy, pp. 2521–2523 (2008).

[43] W. Fischer et al., "Long-range and Head-on Compensation Studies in RHIC with Lessons for the LHC," Proc. Final CARE-HHH Workshop on Scenarios for the LHC Upgrade and Fair (HHH-2008), Chavannes-de-Bogis, Switzerland; W. Scandale and F. Zimmermann (eds.), CERN-2009-004 (2009); CARE-Conf-08-032-HHH (2008).

[44] N.P. Abreu, W. Fischer, Y. Luo, and G. Robert-Demolaize, "Stochastic Boundary, Diffusion, Emittance Growth and Lifetime Calculation for the RHIC e-Lens," BNL C-A/AP/347 (2009).

[45] A. Valishev, Y. Luo, and W. Fischer, "Summary of the LARP Mini-Workshop on Electron Lens Simulations at BNL," BNL C-A/AP/353 (2009).

[46] Y. Luo, N.P. Abreu, R. de Maria, W. Fischer, G. Robert-Demolaize, and E. McIntosh, "Weak-Strong Simulation of Head-on Beam–Beam Compensation in the RHIC," Proc. 2009 Particle Accelerator Conf., Vancouver, Canada, pp. 94–96 (2009).

[47] W. Fischer, Y. Luo, and C. Montag, "Bunch Length Effects in the Beam–Beam Compensation with an Electron Lens," BNL C-AD/AP/359 (2010).

[48] W. Fischer, Y. Luo, and C. Montag, "Bunch Length Effects in the Beam–Beam Compensation with an Electron Lens," Proc. 2010 Int. Particle Accelerator Conf., Kyoto, Japan, pp. 4755–4757 (2010).

[49] C. Montag, W. Fischer, and D.M. Gassner, "Optimizing the Beam–Beam Alignment in an Electron Lens Using Bremsstrahlung," Proc. 2010 Int. Particle Accelerator Conf., Kyoto, Japan, pp. 537–539 (2010).

[50] W. Fischer et al., "Status of the RHIC Head-on Beam–Beam Compensation Project," Proc. 2010 Int. Particle Accelerator Conf., Kyoto, Japan, pp. 513–515 (2010).

[51] Y. Luo and W. Fischer, "6-D Weak-Strong Simulation of Head-on Beam–Beam Compensation in the RHIC," Proc. 2010 Int. Particle Accelerator Conf., Kyoto, Japan, pp. 4758–4760 (2010).

[52] Y. Luo and W. Fischer, "Simulation Study of Dynamic Aperture with Head-on Beam–Beam Compensation in the RHIC," BNL C-AD/AP/392 (2010).

[53] Y. Luo, W. Fischer, and X. Gu, "Coupling Effect on the Proton Optics From the Electron Lenses," BNL C-AD/AP/395 (2010).

[54] X. Gu, A. Pikin, M. Okamura, W. Fischer, Y. Luo, R. Gupta, J. Hock, A. Jain, and D. Raparia, "RHIC Electron Lens Beam Transport System Design Considerations," BNL C-AD/AP/409 (2010).

[55] X. Gu, Y. Luo, A. Pikin, M. Okamura, W. Fischer, C. Montag, R. Gupta, J. Hock, A. Jain, and D. Raparia, "Effect of the Electron Lenses on the RHIC Proton Beam Closed Orbit," BNL C-AD/AP/424 (2011).

[56] X. Gu, M. Okamura, A. Pikin, W. Fischer, and Y. Luo, "The Effects of Realistic Pancake Solenoids on Particle Transport," Nucl. Instrum. Methods A 637 (2011) 190.

[57] W. Fischer et al., "Status of the RHIC Head-on Beam–Beam Compensation Project," Proc. 2011 Particle Accelerator Conf., New York, USA, pp. 2223–2225 (2011).

[58] Y. Luo, W. Fischer, X. Gu, and A.I. Pikin, "Optimizing the Electron Beam Parameters for Head-on Beam–Beam Compensation in RHIC," Proc. 2011 Particle Accelerator Conf., New York, USA, pp. 70–72 (2011).

[59] A.I. Pikin et al., "Structure and Design of the Electron Lens for RHIC," Proc. 2011 Particle Accelerator Conf., New York, USA, pp. 2309–2311 (2011).

[60] X. Gu, W. Fischer, R.C. Gupta, J. Hock, Y. Luo, M. Okamura, A.I. Pikin, and D. Raparia, "Designing a Beam Transport System for RHIC's Electron Lens," Proc. 2011 Particle Accelerator Conf., New York, USA, pp. 1205–1207 (2011).

[61] X. Gu, W. Fischer, R.C. Gupta, J. Hock, Y. Luo, M. Okamura, A.I. Pikin, and D. Raparia, "The Effects of the RHIC e-Lenses' Magnetic Structure Layout on the Proton Beam Trajectory," Proc. 2011 Particle Accelerator Conf., New York, USA, pp. 1202–1204 (2011).

[62] R.C. Gupta et al., "Magnetic Design of e-Lens Solenoid and Corrector System for RHIC," Proc. 2011 Particle Accelerator Conf., New York, USA, pp. 1130–1132 (2011).

[63] P. Thieberger et al., "Proposed Electron Halo Detector System as One of the Beam Overlap Diagnostic Tools for the New RHIC Electron Lens," Proc. 2011 Particle Accelerator Conf., New York, USA, pp. 489–491 (2011).

[64] C. Montag, M. Bai, K.A. Drees, W. Fischer, A. Marusic, and G. Wang, "Beam Experiments Related to the Head-on Beam–Beam Compensation Project at RHIC," Proc. 2011 Particle Accelerator Conf., New York, USA, pp. 2243–2245 (2011).

[65] P. Thieberger et al., "Design of a Proton-Electron Beam Overlap Monitor for the New RHIC Electron Lens, Based on Detecting Energetic Backscattered Electrons," Proc. Beam Instrumentation Workshop BIW12, Newport News, Virginia, USA (2012).

[66] T.A. Miller, J. Aronson, D.M. Gassner, and A. Pikin, "RHIC Electron Lens Beam Profile Monitoring," Proc. Beam Instrumentation Workshop BIW12, Newport News, Virginia, USA (2012).

[67] W. Fischer et al., "Construction Progress of the RHIC Electron Lenses," Proc. 2012 Int. Particle Accelerator Conf., New Orleans, Louisiana, USA, pp. 2125–2127 (2012).

[68] X. Gu et al., "The e-Lens Test Bench for RHIC Beam–Beam Compensation," Proc. 2012 Int. Particle Accelerator Conf., New Orleans, Louisiana, USA, pp. 2720–2722 (2012).

[69] X. Gu, W. Fischer, D.M. Gassner, K. Hamdi, J. Hock, Y. Luo, C. Montag, M. Okamura, A.I. Pikin, and P. Thieberger, "A Split-Electrode for Clearing Scattered Electrons in the RHIC e-Lens," Proc. 2012 Int. Particle Accelerator Conf., New Orleans, Louisiana, USA, pp. 4038–4040 (2012).

[70] Y. Luo, W. Fischer, N.P. Abreu, A. Pikin, and G. Robert-Demolaize, "Six-Dimensional Weak-Strong Simulation of Head-on Beam–Beam Compensation in the Relativistic Heavy Ion Collider," Phys. Rev. ST Accel. Beams 15 (2012) 051004.

[71] S.M. White, W. Fischer, and Y. Luo, "Simulations of Coherent Beam–Beam Effects with Head-on Compensation," Proc. 2012 Int. Particle Accelerator Conf., New Orleans, Louisiana, USA, pp. 187–189 (2012).

[72] T.A. Miller, J.N. Aronson, D.M. Gassner, X. Gu, A.I. Pikin, and P. Thieberger, "Electron Lens Test Stand Instrumentation Progress," Proc. 2012 Int. Beam Instrumentation Conf., Tsukuba, Japan (2012).

[73] X. Gu et al., "RHIC Electron Lens Test Bench – High Intensity Electron Beam Characteristics and Hardware Commissioning," report in preparation (2013).

[74] D.M. Gassner, E. Beebe, W. Fischer, X. Gu, K. Hamdi, J. Hock, C. Liu, T.A. Miller, A. Pikin, and P. Thieberger, "RHIC Electron Lens Test Bench Diagnostics," Proc. DIPAC2011, Hamburg, Germany, pp. 38–40 (2011).

[75] E. Keil, "Beam–Beam Dynamics," in CERN 95-06, pp. 539–555 (1995).

[76] E.D. Courant and H. Snyder, "Theory of the Alternating-Gradient Synchrotron," Ann. Phys. 281 (1957) 360.

[77] D.A. Edwards and M. Syphers, "Linear Betatron Motion," *Handbook of Accelerator Physics and Engineering*, 3rd printing (Singapore: World Scientific, 2006), 65.

[78] M. Bai, private communication (2011).

[79] G. Kuznezov, BINP Novosibirsk (2011).

[80] A. Jain, "Plans for Measurement of Field Straightness in the Solenoids for the Electron Lens System for RHIC," presentation at 17th International Magnetic Measurement Workshop (IMMW17), Barcelona, Spain (2011).

[81] P. Görgen, O. Boine-Frankenheim, and W. Fischer, "BTF Measurements with Beam–Beam Interactions," these proceedings.